ELSEVIER

International Journal of Mass Spectrometry 223–224 (2003) 411–425

International Journal of Mass Spectrometry

www.elsevier.com/locate/ijms

The gas-phase chemistry of iron cations coordinated to benzene and the extended aromatic coronene

Doina Caraiman, Diethard K. Bohme*

Department of Chemistry, Center for Research in Mass Spectrometry and Center for Research in Earth and Space Science, York University, 124 CCB, 4700 Keele Street, Toronto, Ont., Canada M3J 1P3

Received 14 January 2002; accepted 24 May 2002

Abstract

Fe^+ has been coordinated to benzene and the extended aromatic coronene molecule in helium bath gas at 0.35 ± 0.01 Torr and 295 ± 2 K within a Selected-Ion Flow Tube (SIFT) tandem mass spectrometer. Rates were measured for reactions of the bare Fe^+ ion, the $C_6H_6Fe^+$ adduct and the $C_{24}H_{12}Fe^+$ adduct with D_2, N_2, CO_2, CH_4, C_2H_2, C_2H_4, SO_2, C_6D_6, NH_3, H_2O and CO. Comparisons of measured rates indicate that the presence of benzene and coronene leads to enhancements in the reactivity of bare Fe^+ by up to five orders of magnitude. Ligation and sequential ligation was the only chemistry observed with most of the ligands investigated and the observed extent of ligation was employed to determine coordination numbers and these were rationalized in terms of the modes of coordination of Fe^+ with the (flat) aromatic substrate and the ligand. However, bimolecular oxidation channels were observed to compete with ligation in the reactions with N_2O and O_2. The oxidation of Fe^+ to form FeO^+ with N_2O was observed to be catalyzed by the presence of benzene or coronene. Fe-atom abstraction to form FeO_2 was observed in the reactions with O_2. The $C_6H_6Fe^+$ adduct also eliminated water upon addition of O_2 to form a benzometalcycle cation, $FeC_6H_4O^+$, and was observed to be able to initiate the Fe^+ catalyzed oxidation of benzene to 1,2-dihydroxybenzene (catechol). (Int J Mass Spectrom 223–224 (2003) 411–425)

Keywords: Iron cation; Benzene; Coronene; Ligation

1. Introduction

The thermochemistry and structures of metal cation-π interactions are receiving increasing attention in recent years, particularly interactions with benzene and other aromatic molecules as substrates [1–8]. For example, benzene has become a prototype aromatic molecule in the study of cation-interactions that determine the structures of biomolecules [5,9]. Remarkable multi-decker sandwiches and "rice ball" complexes have been identified for transition metals interacting with benzene in the gas phase [10,11]. Coronene, a larger π system, is a good model molecule for graphite [12]. Gas-phase measurements at low pressures have explored the formation and strengths of the interactions of 25 different metal ions with this molecule to form both the monomer and dimer complexes [13]. Also there is increasing interest in the role of metal ion interactions with benzene and polycylic aromatic hydrocarbons in interstellar chemistry in which these large molecules can contribute to the depletion of atomic ions in the interstellar medium and

* Corresponding author. E-mail: dkbohme@science.yorku.ca

1387-3806/02/$ – see front matter
PII S1387-3806(02)00933-8

can act as platforms for catalytic gas-phase chemistry [14,15].

The bonding of transition metal cations with aromatic systems, benzene in particular, has been intensely studied both experimentally and theoretically [6–8]. The bonding is described as being predominantly electrostatic, with an important contribution of promotion, hybridization, orientation of the singly or doubly occupied d orbitals on the metal ion and metal d to π^* donation [6]. The electrostatic components to the bonding in $C_6H_6Fe^+$ are the charge-induced dipole and charge quadrupole. Metal d donation into π^* antibonding orbitals of benzene significantly increases the binding energy. Promotion to the ^{4}F state of Fe^+ has been found to enhance the electrostatic binding by reducing the metal–ligand repulsion and decreasing the metal–ligand distance. This promotion also increases the metal to ligand dative interaction by increasing the number of 3d electrons available for donation and increases the d orbital overlap with the benzene π^* orbitals [16].

MCPF calculations [6], indicate that $C_6H_6Fe^+$ has C_{6v} symmetry, with the metal cation situated along the C_6 axis of benzene. The bond-dissociation energy calculated with respect to the ^{4}F excited state of Fe^+ is 56.8 kcal mol^{-1}. When accounting for the promotion energy from the ^{6}D ground state of Fe^+ to the excited state ^{4}F, a bond-dissociation energy of 51.1 kcal mol^{-1} is obtained with respect to the ground state of Fe^+. These results are in good agreement with B3LYP calculations, [8] that indicate a binding energy of 51.5 kcal mol^{-1} (corrected for the promotion energy). A C_{2v} symmetry for the $C_6H_6Fe^+$ complex resulted from a modest boat-shaped Jahn-Teller distortion of the benzene ring with the 2-fold C atoms bending toward the metal ion. The most recent and probably most accurate experimental value for $D_0(C_6H_6\text{-}Fe^+)$ is 49.6 ± 2.3 kcal mol^{-1} as obtained from threshold dissociation using guided-ion beam mass spectrometry by Meyer et al. [7].

With its larger polarizability (38 Å^3 vs. 10.32 Å^3 for benzene) coronene is expected to form stronger electrostatic complexes than benzene [13]. Experimentally, photodissociation of mixed ligand sandwich complexes $[A_x\text{–Fe–}B_y]^+$ with A and B benzene, coronene or C_{60} and $x + y = 1$ or 2 indicated that the relative strength of ligand binding to iron cation is C_{60} < benzene < coronene [17]. Recent B3LYP/DFT calculations determined structures and binding energies of first-row transition metal cations bonded to coronene [18]. The most stable Fe^+-coronene adduct was found to have C_{2v} symmetry and a binding energy of 56.0 kcal mol^{-1}, just slightly larger than the calculated binding energy for Fe^+-benzene [18]. However, only coordination with the central ring was investigated in these calculations. Earlier extended Hückel and SCF-MS-X_α theoretical calculations predicted that, upon being trapped by coronene in a C_{6v} structure, the iron cation could migrate toward an outer ring with which it should be more tightly bound [19]. Such a result is in agreement with calculated nucleus-independent chemical shifts (NICS) that suggest that the central ring in coronene has diminished aromatic character, but the peripheral rings are fully aromatic, therefore better binding sites for cationic species [20].

Although much is known about the nature of $C_6H_6Fe^+$ and $C_{24}H_{12}Fe^+$ adduct ions, their chemical reactivities are still relatively unexplored. We have reported previously the reactivity of $C_6H_6Fe^+$ with N_2O and CO in a comparative study directed toward elucidating the bonding of Fe^+ to C_{60} [21]. Also, FT-ICR measurements have been reported for the reactions of $C_6H_6Fe^+$ with N_2O and O_2 in a study of oxidation chemistry [22,23]. Very recently molecular beam/time-of-flight mass spectrometry has been used to explore the interaction of $C_6H_6Fe^+$ with coronene and C_{60} in a study of competitive binding in mixed ligand sandwich complexes [17].

Here we report the first systematic investigation of the chemical reactivity of thermalized $C_6H_6Fe^+$ and $C_{24}H_{12}Fe^+$. We have chosen a wide range of small, primarily inorganic, molecules as chemical reagents. These include N_2, D_2, CO_2, CH_4, SO_2, C_2H_4, C_2H_2, H_2O, NH_3, CO, C_6D_6, N_2O and O_2 which are the same as those used by us recently to probe the influence of curvature on the ligation and reactivities of corannulene·Fe^+ and C_{60}·Fe^+ [24]. In this earlier study we found that the presence of either corannulene

or C_{60} enhances the reactivity of bare Fe^+ by up to five orders of magnitude. The present comparative study intends to identify similarities and differences in the reactivity of free iron cations and iron cations coordinated to benzene and the extended flat aromatic coronene molecule.

2. Experimental

Iron-benzene and iron-coronene adduct ions were generated by attaching Fe^+ to the respective aromatic molecule in a flowing He bath gas. This was achieved using a Selected-Ion Flow Tube (SIFT) apparatus that has been described in detail previously [25].

The reactant Fe^+ was generated from pure ferrocene, $(c\text{-}C_5H_5)_2Fe$, vapor in a low pressure ionization source by 70 eV electron-impact dissociative ionization. Fe^+ ions were mass selected from the ions produced in this source with a quadrupole mass filter and then injected into the flow tube containing He buffer gas maintained at a pressure of 0.35 ± 0.01 Torr and room temperature, 295 ± 2 K. Neutral benzene or coronene was added upstream of the flow tube and the amount of benzene added was held constant with a needle valve. Under these conditions Fe^+ was observed to react with benzene sequentially to add two benzene molecules, presumably by termolecular collisional association (rather than by radiative association). The flow of benzene was adjusted to optimize the downstream signal of the first adduct ion. No electron transfer was observed between benzene (IE $= 9.24378 \pm 0.00007$ eV), [26] and Fe^+ (IE(Fe) $= 7.9024 \pm 0.0001$ eV), [26] since it is endothermic. Coronene vapor was added directly from a heated stainless-steel tubular inlet maintained at a fixed temperature of about 200 °C. The first and second adducts of Fe^+ with coronene also were produced sequentially along with coronene$^+$ since electron transfer is exothermic in this case (IE(coronene) $= 7.29 \pm 0.03$ eV) [26]. The flow of coronene could not be adjusted for optimum adduct formation but the first adduct was predominant at the sublimation temperature employed: the ion-signal ratios Fe^+:$C_{24}H_{12}Fe^+$:(coronene)$_2Fe^+$:coronene$^+$ were observed downstream to be approximately 7:1:0.01:3.

Pursuant to their formation, the Fe^+ adduct ions were allowed to thermalize before entering the reaction region still further downstream where the neutral reagent was added. Reactant and product ions were monitored still further downstream with a second quadrupole mass filter as a function of the neutral reagent flow. Rate coefficients for the primary reactions were determined in the usual manner from the rate of decay of the reactant ion intensity with added neutral reagent (with an uncertainty estimated to be less than ±30%). Rate coefficients for secondary and higher-order reactions could be obtained by fitting the experimental data to solutions of differential equations for successive reactions. Measured branching ratios (percentages) for primary reactions with more than one product are rounded off to the nearest 5 in the second digit.

Previous studies by Viggiano and co-workers have shown that weakly ligated cluster ions (with binding energies lower than 13 kcal mol^{-1}) can undergo thermal dissociation in high-pressure flow-tube instruments [27]. In our instrument weak ligation can also be discriminated against in the sampling process due to collisional dissociation resulting from the presence of a small electric field at the nose cone that is biased at ca. −7 V. Previous experience in our laboratory indicates that ligand binding energies must be ca. 10 kcal mol^{-1} for the ligated species to survive thermal dissociation and dissociation upon sampling.

The multi-collision induced dissociation (CID) of sampled ions can be investigated by raising the potential of the sampling nose cone from −4 to −80 V [28]. Thresholds for dissociation are obtained from plots of relative ion intensities as a function of accelerating voltage and these provide information on bond connectivities and relative binding energies. They do not provide absolute thermochemical information since both dissociation and addition can proceed under multicollision conditions.

The coronene (99% purity) and benzene (99.9% HPLC grade) were both purchased from Sigma Aldrich. Benzene-d_6 with minimum 98% D isotopic

purity was obtained from MSD isotopes and was used when necessary to distinguish between interfering ions or to clearly identify ions separated by one or two mass units.

Reactant neutrals were introduced into the reaction region either as a pure gas, as a mixture in helium, or as vapors diluted in helium to various levels (H_2O and C_6D_6). All neutrals (except for de-ionized water) were obtained commercially and were of high purity (>99.5%); the neutral reagents were used without further purification, except for the liquid compounds that were subjected to multiple freeze–pump–thaw cycles to remove non-condensable gases.

3. Results and discussion

3.1. Sequential ligation

With the exception of the N_2O and O_2 chemistry (presented separately), the chemistry initiated by $C_6H_6Fe^+$ and $C_{24}H_{12}Fe^+$ with the molecules investigated was observed to be dominated by sequential ligation reactions of type (1).

$$C_xH_yFeL_n{}^+ + L + He \rightarrow C_xH_yFeL_{n+1}{}^+ + He \quad (1)$$

Here $(x, y) = (6, 6)$ and $(24, 12)$ and $n = 1$–3. Under the adopted experimental conditions, each step in these sequences is expected to proceed by termolecular association in which helium is acting as a third body to stabilize the intermediate adducts. An overview of the kinetic results obtained for the sequential ligation of $C_6H_6Fe^+$ and $C_{24}H_{12}Fe^+$ is presented in Table 1 along with results obtained previously for corresponding reactions with Fe^+ [24,29–31]. The reaction efficiencies in Table 1 are expressed as the ratio of the measured rate coefficient, k_{obs}, and the collision rate coefficient, k_c, calculated using the algorithm of the combined variational transition-state theory developed by Su and Chesnavich [32].

The number of molecules seen to attach to benzene-Fe^+ and coronene-Fe^+ under the SIFT conditions differs from neutral to neutral. One molecule of D_2, N_2, CO_2, SO_2, C_2H_4 and C_6D_6 and two molecules of CH_4, C_2H_2, H_2O, CO were observed to add to both benzene-Fe^+ and coronene-Fe^+ in the flow range investigated. Ammonia was observed to attach twice to $C_6H_6Fe^+$ and three times to $C_{24}H_{12}Fe^+$.

Almost all of the addition reactions were seen to be reversible. This reversibility was exhibited as curvature in the semi-logarithmic decay of an ion or as an approach to, or attainment of, equilibrium in the ratio plots of $[C_xH_yFeL_{n+1}{}^+]/[C_xH_yFeL_n{}^+]$ vs. the flow of ligand, L. This is illustrated in Fig. 1 for the ligation reactions (2)–(5) with N_2 and CO_2.

$$C_6H_6Fe^+ + N_2 + He \rightarrow C_6H_6FeN_2{}^+ + He \quad (2)$$

$$C_6H_6Fe^+ + CO_2 + He \rightarrow C_6H_6FeCO_2{}^+ + He \quad (3)$$

$$C_{24}H_{12}Fe^+ + N_2 + He \rightarrow C_{24}H_{12}FeN_2{}^+ + He \quad (4)$$

$$C_{24}H_{12}Fe^+ + CO_2 + He \rightarrow C_{24}H_{12}FeCO_2{}^+ + He \quad (5)$$

The semi-logarithmic decays of $C_{24}H_{12}Fe^+$ in its reaction with N_2 and CO_2 both exhibit curvature and the product to reactant ion signal ratio plots show approach to, and attainment of, equilibrium. The data for the corresponding reactions with $C_6H_6Fe^+$ are similar, but the reactions are slower and the decays are less developed. Analysis of reversible kinetics indicates that about one order-of-magnitude of decay is required for the initial slope of the semi-logarithmic decay of the primary ion to provide a rate coefficient within 10% of its true value; less linearity will provide a rate coefficient that should be regarded as a lower limit. We have adopted this approach in the analysis of all our data for reactions leading to a single adduct ion (D_2, N_2, CO_2, SO_2, C_2H_4 and C_6D_6). In the absence of at least one order-of-magnitude decay, the curvature in the semi-logarithmic decay may be fitted by taking into account a reverse reaction to provide a better value for the forward pseudo second-order rate coefficient, k_f, for ligation and a value for the reverse pseudo first-order rate coefficient, k_r, for de-ligation. The ratio k_f/k_r will provide a measure of the equilibrium constant K (standard state = 1 atm).

The equilibrium constant may also be determined from a plot of the product-to-reactant ion signal

Table 1
Summary of measured rate coefficients (k_{obs}, $cm^3\,molecule^{-1}\,s^{-1}$), reaction efficiencies (k_{obs}/k_c with k_c: the collision rate coefficient calculated using the algorithm of the combined variational transition-state theory developed by Su and Chesnavich [32]) and observed product ions for reactions of Fe^+, $C_6H_6Fe^+$ and $C_{24}H_{12}Fe^+$ and with ligand molecules L occurring in He at 0.35 ± 0.01 Torr and 295 ± 2 K

Ligand	FeL_n^+	k_{obs}	$C_6H_6FeL_n^+$	k_{obs}	k_{obs}/k_c	$C_{24}H_{12}FeL_n^+$	k_{obs}	k_{obs}/k_c
D_2	–[a]	$<10^{-13}$	$C_6H_6FeD_2^+$	1.0×10^{-10}	0.07	$C_{24}H_{12}FeD_2^+$	1.9×10^{-10}	0.14
N_2	–[a]	$<10^{-14}$	$C_6H_6FeN_2^+$	1.5×10^{-10}	0.23	$C_{24}H_{12}FeN_2^+$	2.5×10^{-10}	0.41
CO_2	–[a]	$<10^{-15}$	$C_6H_6FeCO_2^+$	6.0×10^{-11}	0.09	$C_{24}H_{12}FeCO_2^+$	5.0×10^{-10}	0.78
CH_4	$FeCH_4^+$ [b]	$<5.0 \times 10^{-14}$	$C_6H_6FeCH_4^+$ $C_6H_6Fe(CH_4)_2^+$	3.3×10^{-10} 3.3×10^{-12}	0.33	$C_{24}H_{12}FeCH_4^+$ $C_{24}H_{12}Fe(CH_4)_2^+$	7.7×10^{-10} 5.3×10^{-12}	0.80
SO_2	$FeSO_2^+$ [c] $Fe(SO_2)_2^+$ $Fe(SO_2)_3^+$	8.1×10^{-12} 1.4×10^{-9} 1.2×10^{-9}	$C_6H_6FeSO_2^+$	6.3×10^{-10}	0.49	$C_{24}H_{12}FeSO_2^+$	7.1×10^{-10}	0.57
C_2H_4	$FeC_2H_4^+$ [b] $Fe(C_2H_4)_2^+$ $Fe(C_2H_4)_3^+$ $Fe(C_2H_4)_4^+$	6.1×10^{-11} 6.3×10^{-10} 8.7×10^{-11} 3.0×10^{-13}	$C_6H_6FeC_2H_4^+$	7.0×10^{-10}	0.67	$C_{24}H_{12}FeC_2H_4^+$	6.6×10^{-10}	0.67
C_2H_2	$FeC_2H_2^+$ [b] $Fe(C_2H_2)_2^+$ $Fe(C_2H_2)_3^+$ $Fe(C_2H_2)_4^+$ $Fe(C_2H_2)_5^+$	1.6×10^{-11} 7.7×10^{-10} 7.6×10^{-10} 2.0×10^{-12} 5.0×10^{-12}	$C_6H_6FeC_2H_2^+$ $C_6H_6Fe(C_2H_2)_2^+$	5.0×10^{-10}	0.55	$C_{24}H_{12}FeC_2H_2^+$ $C_{24}H_{12}Fe(C_2H_2)_2^+$	4.7×10^{-10} 3.4×10^{-12}	0.54
H_2O	–[a]	$<10^{-13}$	$C_6H_6FeH_2O^+$ $C_6H_6Fe(H_2O)_2^+$	3.2×10^{-10} 1.1×10^{-11}	0.15	$C_{24}H_{12}FeH_2O^+$ $C_{24}H_{12}Fe(H_2O)_2^+$	5.3×10^{-10} 4.8×10^{-11}	0.25
NH_3	$Fe(NH_3)^+$ [d] $Fe(NH_3)_2^+$ $Fe(NH_3)_3^+$ $Fe(NH_3)_4^+$	1.7×10^{-11} 1.0×10^{-9} 8.2×10^{-12} $<5 \times 10^{-14}$	$C_6H_6FeNH_3^+$ $C_6H_6Fe(NH_3)_2^+$	7.0×10^{-10} 2.0×10^{-10}	0.37	$C_{24}H_{12}FeNH_3^+$ $C_{24}H_{12}Fe(NH_3)_2^+$ $C_{24}H_{12}Fe(NH_3)_3^+$	8.0×10^{-10} 8.5×10^{-10} 2.7×10^{-11}	0.41
CO	–[a]	$<10^{-14}$	$C_6H_6FeCO^+$ $C_6H_6Fe(CO)_2^+$	2.5×10^{-10} 4.5×10^{-11}	0.36	$C_{24}H_{12}FeCO^+$ $C_{24}H_{12}Fe(CO)_2^+$	3.9×10^{-10} 1.2×10^{-10}	0.59
C_6D_6	$FeC_6D_6^+$ [b] $Fe(C_6D_6)_2^+$	9.0×10^{-10} 7.3×10^{-10}	$C_6H_6FeC_6D_6^+$	7.3×10^{-10}	0.68	$C_{24}H_{12}FeC_6D_6^+$	5.8×10^{-10}	0.64

[a] Results from [29].
[b] Results from [30].
[c] Results from [24].
[d] Results from [31].

ratio against the flow of reactant (see Fig. 1). Attainment of equilibrium is manifested in such a plot by linearity since the equilibrium constant $K = [C_xH_yFeL^+]/([C_xH_yFe^+][L])$. An evaluation of K provides a measure of the standard free energy for the ligation reaction, ΔG°, since $\Delta G^\circ = -RT \ln K$. An evaluation of a lower limit to K provides a measure of an upper limit for ΔG°. Table 2 provides values for K and ΔG° obtained for some of the ligation reactions investigated in this study.

Fig. 2 presents data for the sequential ligation of $C_6H_6Fe^+$ and $C_{24}H_{12}Fe^+$ with two CO molecules and is representative of the sequential ligation observed with two ligand molecules (CH_4, C_2H_2, H_2O, CO). The first ligated $C_xH_yFeL^+$ ion now acts as an intermediate reacting further to produce $C_xH_yFeL_2^+$. The $[C_xH_yFeL^+]/([C_xH_yFe^+]$ ratio plot at higher flows of the ligand is modified as a consequence.

Fig. 3 shows data for the special case of ammonia with which two ligand additions were seen for

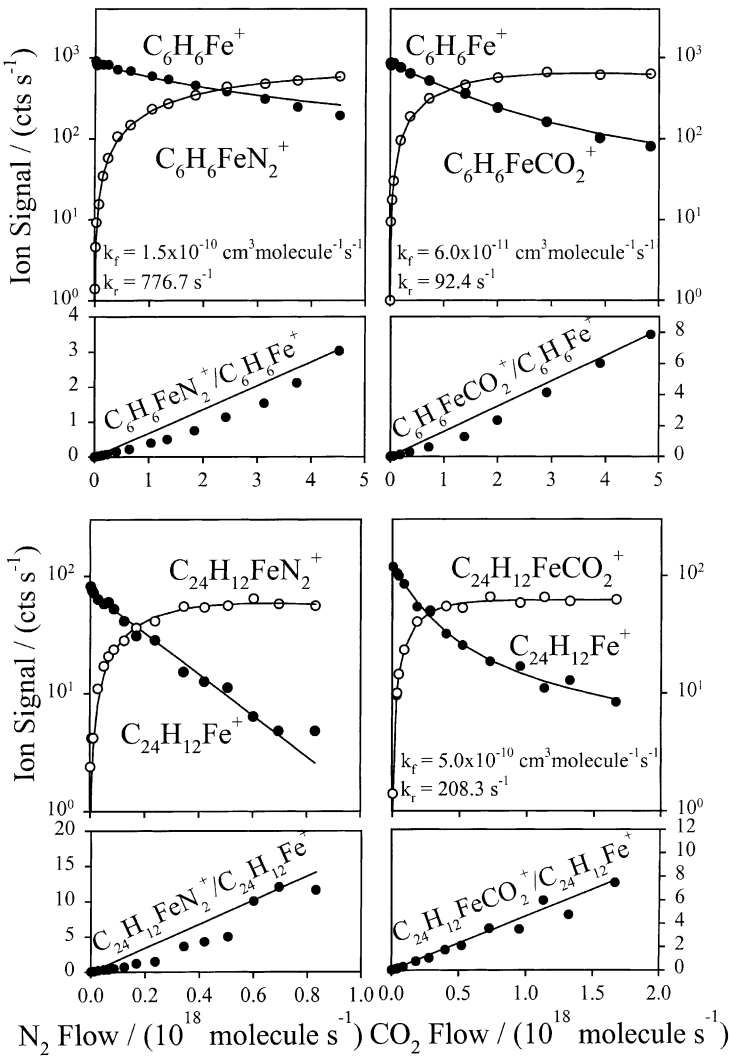

Fig. 1. Kinetic data and ion signal ratio plots for the single ligation reactions of $C_6H_6Fe^+$ and $C_{24}H_{12}Fe^+$ with N_2 and CO_2. The solid lines through the kinetic data represent fits using the solution of the differential equation that describes the reversible ligation. Values determined for forward pseudo second-order rate coefficients, k_f, for ligation and for reverse pseudo first-order rate coefficients, k_r, for de-ligation are also included. The occurrence of the reverse reaction for $C_{24}H_{12}Fe^+$ reacting with N_2 has been neglected in the kinetic analysis.

$C_6H_6Fe^+$ while three ligand additions were seen for $C_{24}H_{12}Fe^+$. The second addition to $C_6H_6Fe^+$ is seen to approach equilibrium while the third addition to $C_{24}H_{12}Fe^+$ is seen to achieve equilibrium.

3.1.1. Rate of ligation

The kinetic results in Table 1 clearly show that the ligation of Fe^+ with benzene or coronene dramatically increases reaction rates, by up to five orders of magnitude, and somewhat more with coronene. These results can be understood in terms of variations in the lifetimes of the intermediate due to changes in the number of degrees of freedom in the intermediate. Ligation reactions proceed in two steps: reversible formation of an intermediate and collisional stabilization of this intermediate by He atoms. The lifetime

Table 2
Results of equilibrium analyses for ligation reactions initiated by $C_6H_6Fe^+$ and $C_{24}H_{12}Fe^+$

Ligand	$C_6H_6Fe^+$		$C_{24}H_{12}Fe^+$	
	K[a]	ΔG° (kcal mol^{-1})[b]	K[a]	ΔG° (kcal mol^{-1})[b]
D_2	2.1×10^5 (3.3×10^6)	−7.2 (−8.9)	5.9×10^6 (1.2×10^7)	−9.2 (−9.7)
N_2	4.0×10^6 (3.3×10^6)	−9.0 (−8.9)	1.2×10^8	−11.0
CO_2	1.3×10^7 (1.6×10^7)	−9.7 (−9.8)	3.4×10^7 (6.1×10^7)	−10.3 (−10.6)
CH_4	$K_1 > 1.7 \times 10^7$ (1.2×10^7) $K_2 = 2.1 \times 10^4$	−9.8 (−9.7) −5.9	$K_1 = 6.6 \times 10^7$ (8.6×10^7) $K_2 = 4.8 \times 10^4$	−10.7 (−10.7) −6.4
SO_2	1.6×10^8	−11.2	9.5×10^8	−12.2
H_2O	$K_1 > 1.8 \times 10^8$ $K_2 = 1.0 \times 10^6$	<−11.3 −8.2	$K_1 > 8.1 \times 10^8$ $K_2 = 1.5 \times 10^6$	<−12.1 −8.4
NH_3	$K_1 > 1.9 \times 10^8$ $K_2 > 9.0 \times 10^7$	<−11.3 <−10.8	$K_1 > 1.0 \times 10^9$ $K_2 > 1.3 \times 10^9$ $K_3 > 6.5 \times 10^7$	<−12.3 <−12.4 <−10.7
CO	$K_3 > 6.6 \times 10^7$ $K_1 > 2.2 \times 10^7$	<−10.7 <−10.0	$K_1 > 7.7 \times 10^7$ $K_2 > 8.9 \times 10^7$	<−9.4 <−10.8
C_2H_4	2.6×10^9	−12.8	5.9×10^8	−12.0
C_2H_2	$K_1 = 8.0 \times 10^8$ $K_2 = 3.6 \times 10^4$	−12.1 −4.8	$K_1 = 5.6 \times 10^8$ $K_2 = 1.0 \times 10^5$	−11.9 −6.8
C_6H_6	$>5.6 \times 10^{10}$	<−14.7	2.1×10^9	−12.7

[a] K is the equilibrium constant (standard state = 1 atm) determined from the ion signal ratio plots that achieved linearity and has an estimated uncertainty up to ±30%; lower limits of K are determined from ratio plots that did not achieve linearity; the values of k_f/k_r (standard state = 1 atm) in parentheses are derived from the ratio of rate coefficients for the forward and reverse reactions obtained by curve fitting the primary ion decay using the solution of the differential equation that describes the reversible ligation. Values of k_f/k_r have an estimated uncertainty up to ±50%. K_1 and K_2 refer to the first and second ligation steps, respectively.

[b] ΔG° is the standard free energy for the ligation reactions calculated as $-RT\ln K$; an evaluation of a lower limit to K provides a measure of an upper limit for ΔG°. The estimated uncertainty in ΔG° derived from K is less than 0.3 kcal mol^{-1} and that derived from k_f/k_r (values in brackets) is less than 0.5 kcal mol^{-1}.

of the intermediate against dissociation back to reactants is dependent on both the degrees of freedom effective in intramolecular energy redisposition in the transient intermediate and its attractive well depth [33]. The actual differences in the attractive well depth for ligation for the systems investigated are not known but certainly, a dramatic increase in the effective degrees of freedom is expected upon ligation with benzene and coronene, and slightly more so with coronene.

3.1.2. Site of ligation

Of course, questions arise regarding the coordination site: where do incoming ligands attach on the $C_6H_6Fe^+$ and $C_{24}H_{12}Fe^+$ adducts, to the metal or to the C_6H_6 or $C_{24}H_{12}$ surface? Since incoming ligands are likely to seek out the site of the charge, we need to consider the extent of intramolecular charge transfer upon Fe^+-adduct formation. The ionization energy of iron (IE = 7.9024 ± 0.0001 eV) is much smaller than that of benzene (9.24378 ± 0.00007 eV) so that intramolecular charge transfer is not expected to occur. Consequently, incoming ligands should attack the Fe^+ site in $C_6H_6Fe^+$. In contrast, IE(Fe) is 0.6 eV higher than that of coronene (IE = 7.29 ± 0.03 eV) so that some charge delocalization onto the carbonaceous surface may occur in this case. Our CID experiments (see Fig. 4) are consistent with such an interpretation: $C_6H_6Fe^+$ dissociates by loss of neutral benzene while $C_{24}H_{12}Fe^+$ dissociates by loss of neutral metal. We

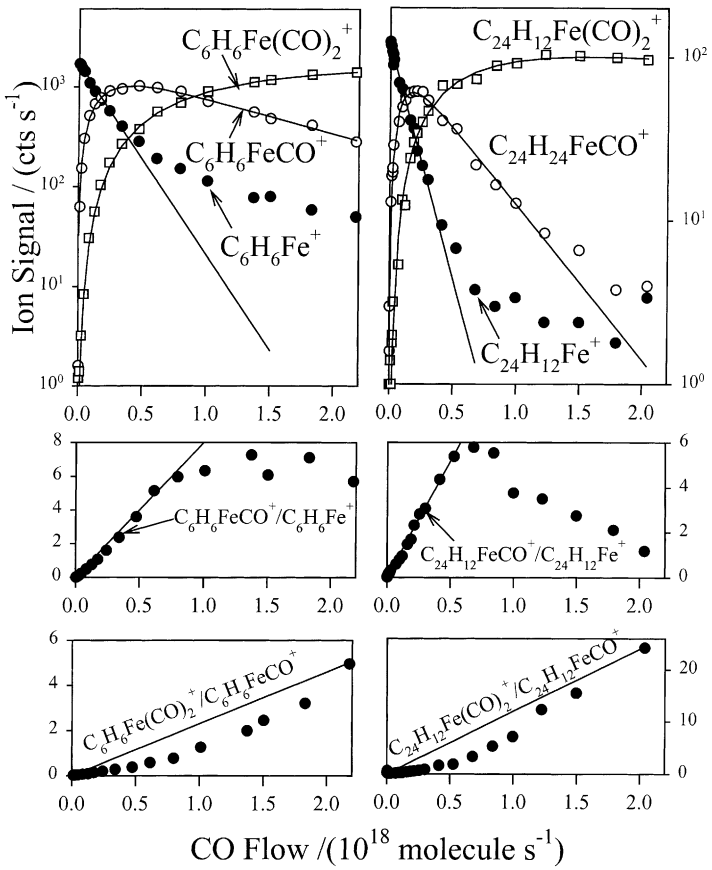

Fig. 2. Kinetic data and ion signal ratio plots for the sequential ligation reactions of $C_6H_6Fe^+$ and $C_{24}H_{12}Fe^+$ with CO. The solid lines through the kinetic data represent fits using the solutions of the differential equations that describes the sequential ligation. The occurrence of reverse reactions has been neglected in the kinetic analysis.

therefore consider that the site of ligation in $C_6H_6Fe^+$ is the metal center and not the carbonaceous surface. The site of ligation of $C_{24}H_{12}Fe^+$ is less certain since ligation of the surface may become possible due to charge delocalization.

3.1.3. Coordination numbers

Notwithstanding the possibility that higher-order addition could be discriminated against experimentally in the case of weak ligands due to thermal dissociation or dissociation in sampling, the number of ligands that were observed to add with measurable rates should provide an indication of the coordination number of the adduct ion. For sequential ligation the first significant drop in the rate of ligation signals the attainment of coordinative saturation. Thus coordination numbers of 1 are assigned for both $C_{24}H_{12}Fe^+$ and $C_6H_6Fe^+$ with N_2, D_2, CO_2, SO_2, C_2H_4 and C_6D_6 and coordination numbers of 2 with CH_4, C_2H_2, H_2O, CO. These coordination numbers can be rationalized in terms of differences expected in the nature and strength of the ligand-metal bonding.

In a previous work [24] we determined coordination numbers for $C_{60}Fe^+$ and $C_{20}H_{10}Fe^+$ from sequential ligation reactions with the same set of neutral molecules used in the present work. We found that these two adduct ions exhibited different coordination numbers with the same ligand and this difference

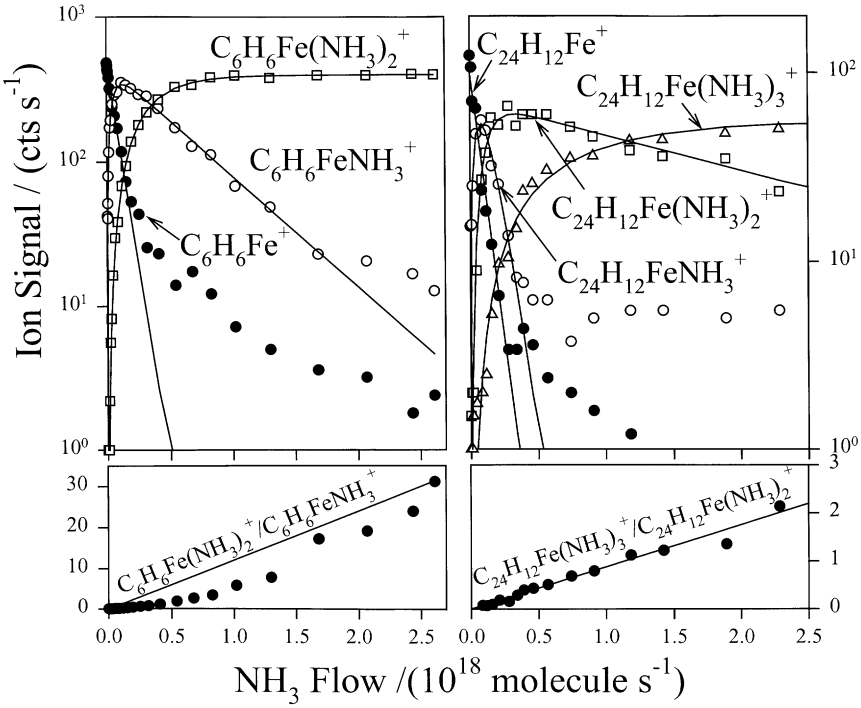

Fig. 3. Kinetic data and ion signal ratio plots for the sequential ligation reactions of $C_6H_6Fe^+$ and $C_{24}H_{12}Fe^+$ with ammonia. The solid lines through the kinetic data represent fits using the solutions of the differential equations that describes the sequential ligation. The occurrence of reverse reactions has been neglected in the kinetic analysis.

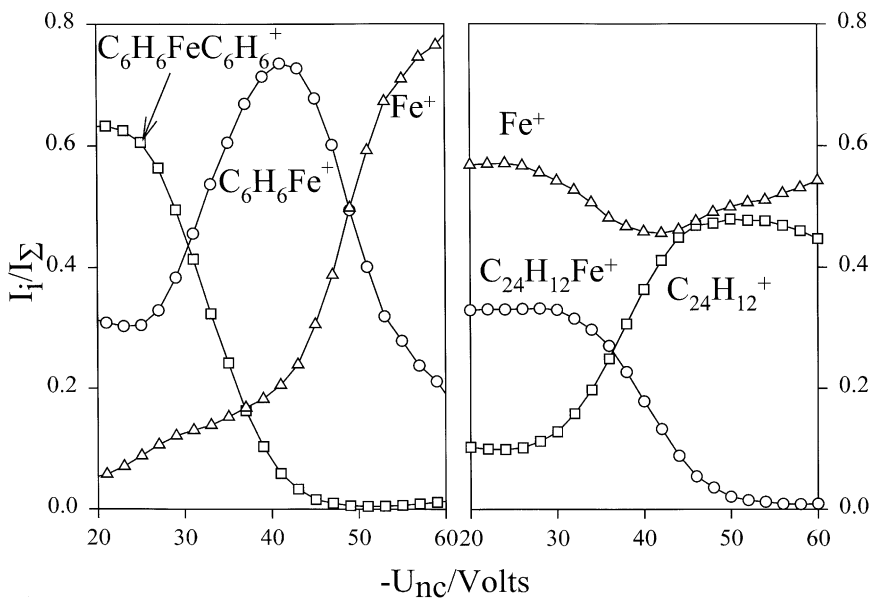

Fig. 4. Profiles obtained for the multi-collision induced dissociation of $C_6H_6Fe^+$ and $C_{24}H_{12}Fe^+$ in Ar at 0.094 Torr.

was attributed to differences in the Fe^+ binding mode arising from differences in the curvature of the carbonaceous surfaces. In contrast, the $C_6H_6Fe^+$ and $C_{24}H_{12}Fe^+$ adducts investigated in this work exhibited the same coordination number with the same ligand (except NH_3) indicating a similar coordination pattern of Fe^+ with both benzene and coronene.

The nature of the bonding with the various ligands investigated is variable, as is the ligation energy. Ligands like N_2, CO_2, SO_2 can form either σ or π bonds with Fe^+, but each ligand can contribute only up to two electrons to the bonding. Fe^+ binds in a dihapto manner to the π systems of C_2H_4, C_2H_2 and CO. Both H_2O and NH_3 form electrostatic adducts with Fe^+ by donating their lone pairs to the metal center. D_2 and CH_4 also form electrostatic adducts with Fe^+, but insertion of the metal cation into the C–H bond is also possible [34]. C_6H_6 usually binds in a hexahapto-manner, but a fluxional tetrahapto-coordination has also been suggested [7].

The highest observed coordination number of 2 is achieved with strong ligands like CO, H_2O and C_2H_2, which have high sequential binding energies to Fe^+ (see Table 3 in [24]). They are all two-electron donors and the adducts $C_6H_6FeL_2^+$ and $C_{24}H_{12}FeL_2^+$ are stable 17-electron species, with both benzene and coronene contributing with six electrons to the bonding. The coordination numbers of one determined for N_2, D_2, CO_2, SO_2 and C_2H_4 (although also potentially two-electron donors) indicate that coordinative saturation was not achieved, probably due to low binding energies for the second ligand.

The coordination number of one assigned with C_6H_6 is expected since benzene is a six-electron donor. $C_6H_6FeC_6H_6^+$ and $C_{24}H_{12}FeC_6H_6^+$ are 19-electron species if all ligands contribute six electrons to the bonding. However, the benzene ligand can coordinate in a tetrahapto-manner, generating stable 17-electron species upon attaching to $C_6H_6Fe^+$ or $C_{24}H_{12}Fe^+$ [7]. Addition of a second molecule of benzene to either $C_6H_6FeC_6H_6^+$ or $C_{24}H_{12}FeC_6H_6^+$ would generate unstable complexes.

The two adducts $C_6H_6Fe^+$ and $C_{24}H_{12}Fe^+$ showed a distinctly different behavior only in reactions with ammonia: while two molecules of ammonia added to $C_6H_6Fe^+$, three molecules attached to $C_{24}H_{12}Fe^+$. This result is puzzling. While the final complex obtained after sequential additions of two molecules of ammonia to $C_6H_6Fe^+$ or η^6-$C_{24}H_{12}Fe^+$ would achieve coordinative saturation (a 17e species), a complex with three ammonia molecules coordinated directly to the metal ion would be a 19-electron species and so should not be stable for either $C_6H_6Fe(NH_3)_2^+$ or η^6-$C_{24}H_{12}Fe^+$. Also, hydrogen bonding of the third ammonia molecule with an ammonia ligand already coordinated at the metal should not discriminate between $C_6H_6Fe(NH_3)_2^+$ and η^6-$C_{24}H_{12}Fe(NH_3)_2^+$. It could be that the third molecule of ammonia coordinates to the carbonaceous surface in the case of $C_{24}H_{12}Fe(NH_3)_2^+$. Some of the charge in the Fe^+-coronene adduct may reside on the carbonaceous surface, since coronene is the species with a lower ionization energy than Fe. The bonding may be electrostatic since ammonia has a high polarizability (2.26 $Å^3$, the highest of the ligands investigated) and a high dipole moment (1.47 D, the second highest of the ligands investigated) [35]. A similar behavior was not observed with H_2O since $C_{24}H_{12}Fe^+$ was observed to add only two water molecules. The maximum flow of water used was four times less than that used for the ammonia experiment and the addition of the second water molecule was more than an order of magnitude slower than the addition of the second ammonia molecule.

3.2. Oxidation reactions

3.2.1. Reactions with N_2O

The observed reactions of $C_6H_6Fe^+$ and $C_{24}H_{12}Fe^+$ with N_2O (see Fig. 5) exhibit competing bimolecular channels that involve oxygen-atom transfer, reaction (6a), and simple addition, reaction (6b).

$$C_xH_yFe^+ + N_2O \rightarrow C_xH_yFeO^+ + N_2 \quad (6a)$$

$$C_xH_yFe^+ + He \rightarrow C_xH_yFeN_2O^+ + He \quad (6b)$$

Here $(x, y) = (6, 6)$ and (24, 12). The total rate coefficients for these reactions with N_2O were measured

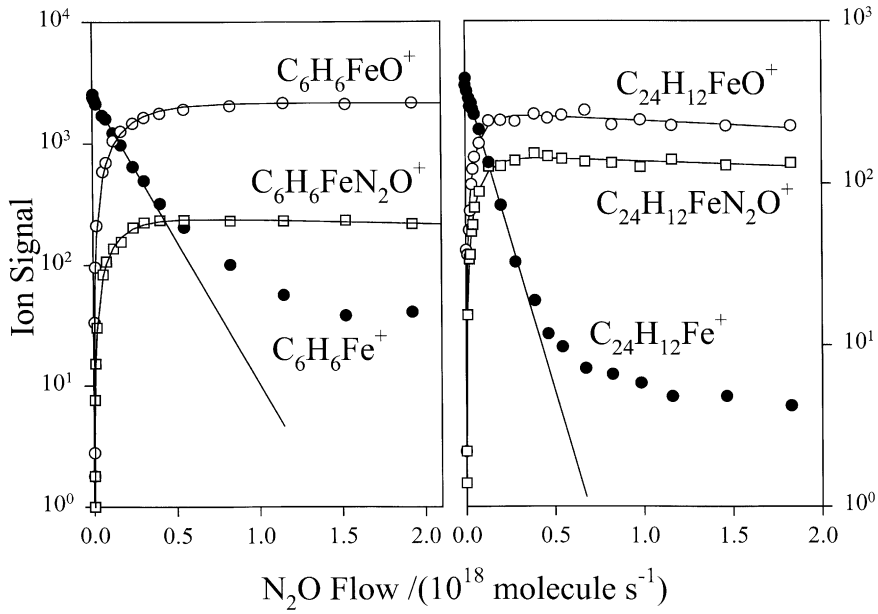

Fig. 5. Experimental data for the reactions of $C_6H_6Fe^+$ and $C_{24}H_{12}Fe^+$ with N_2O. The solid lines represent a fit of the experimental data points with the solution of the system of differential equations appropriate for the observed sequential additions. The occurrence of reverse reactions has been neglected.

to be 2.8×10^{-10} cm^3 molecule^{-1} s^{-1} for $C_6H_6Fe^+$ and 4.7×10^{-10} cm^3 molecule^{-1} s^{-1} for $C_{24}H_{12}Fe^+$. The curvature in the observed semi-logarithmic decays of $C_6H_6Fe^+$ and $C_{24}H_{12}Fe^+$ shown in Fig. 5 is introduced by the occurrence of the reverse reaction (6b). The extent of O-atom transfer was measured to be 90% for $C_6H_6Fe^+$ and 65% for $C_{24}H_{12}Fe^+$ at the He pressure of the experiments. The higher branching ratio for addition of N_2O to $C_{24}H_{12}Fe^+$ is probably due to the higher number of degrees of freedom in coronene. Higher-order chemistry was not observed for any of the observed primary product ions in the flow range investigated.

The occurrence of the oxygen-atom transfer reactions provides lower limits for the oxygen affinities of $C_{24}H_{12}Fe^+$ and $C_6H_6Fe^+$ of 40.0 kcal mol^{-1}, the O-atom affinity of N_2 [36].

The rate coefficients for the O-atom transfer channel with $C_6H_6Fe^+$ and $C_{24}H_{12}Fe^+$ (determined by taking into account the branching ratios for this channel) are both one order of magnitude higher than the rate of O-atom transfer for the reaction of bare Fe^+ with N_2O (3.1×10^{-11} cm^3 molecule^{-1} s^{-1}). The oxidation of Fe^+ to form FeO^+ can therefore be regarded as being "catalyzed" by the presence of benzene or coronene by up to one order of magnitude with the assumption that O-atom transfer leads to the formation of a Fe–O bond in the $C_xH_yFeO^+$ product ion. We have attempted to elucidate this point with multi-collision CID experiments. The ion signals for the reaction of $C_{24}H_{12}Fe^+$ were too low to provide reliable results. Results of CID experiments with $C_6H_6FeO^+$ indicate that this ion may be a 50:50 mixture of FeO^+ attached to benzene and iron cation bonded to C_6H_6O (perhaps phenol). FeO^+ and Fe^+ were both observed to be generated at about the same threshold voltage. However, some uncertainty is introduced by the further dissociation of FeO^+ to produce Fe^+ at only a slightly higher voltage.

The reaction between $C_6H_6Fe^+$ and N_2O has been investigated before with a FT-ICR mass spectrometer [22]. The products $C_6H_6FeO^+$, $C_5H_6Fe^+$ and $Fe(C_6H_4)O^+$ were observed to account for 86, 9 and 5% of the reactive collisions, respectively. The observation of $C_6H_6FeO^+$ is consistent with our

results and the absence of an adduct ion $C_6H_6FeN_2O^+$ is not unexpected, given the much lower pressure of the ICR experiments at which collisional stabilization is much less effective. The formation of $C_5H_6Fe^+$ in the ICR experiments indicates a ring-opening process accompanied by several C–C and C–H bond dissociations, ring rearrangement and loss of CO and N_2. Also, generation of $Fe(C_6H_4)O^+$ requires breaking two C–H bonds. These reaction channels were not observed under our SIFT conditions possibly due to a better thermalization of both Fe^+ prior to addition to benzene and $C_6H_6Fe^+$ prior to the reaction with N_2O. The rate coefficient measured with the ICR reaction is 8.4×10^{-10} cm^3 molecule^{-1} s^{-1}, larger than the collision rate (7.4×10^{-10} cm^3 molecule^{-1} s^{-1}). Our value for comparison is a lower limit, $k \geq 2.8 \times 10^{-10}$ cm^3 molecule^{-1} s^{-1}.

3.2.2. Reactions with O_2

Kinetic profiles for the ion–molecule reactions of $C_6H_6Fe^+$ and $C_{24}H_{12}Fe^+$ with molecular oxygen are presented in Fig. 6.

Oxygen-atom transfer was absent from the reactions with molecular oxygen, presumably because O_2 is a poor O-atom donor, D(O–O) = 119.2 kcal mol^{-1} [36]. Other bimolecular channels were observed to occur instead and these were different for the reactions of $C_6H_6Fe^+$ which exhibited four channels and $C_{24}H_{12}Fe^+$ which exhibited two channels.

Reaction (7a–d) summarizes the channels observed with $C_6H_6Fe^+$. Products were

$$C_6H_6Fe^+ + O_2 \rightarrow FeC_6H_4O^+ + H_2O \quad (7a)$$

$$C_6H_6Fe^+ + O_2 \rightarrow Fe^+ + (C_6H_6O_2) \quad (7b)$$

$$C_6H_6Fe^+ + O_2 \rightarrow C_6H_6{}^+ + FeO_2 \quad (7c)$$

$$C_6H_6Fe^+ + O_2 \rightarrow C_6H_6FeO_2{}^+ \quad (7d)$$

observed in the ratio (7a):(7b):(7c):(7d) = 0.80:0.025:0.025:0.15 with water elimination, channel (7a), being by far the most predominant. Two channels were observed with $C_{24}H_{12}Fe^+$ according to reaction (8) with Fe abstraction, channel (8a), being

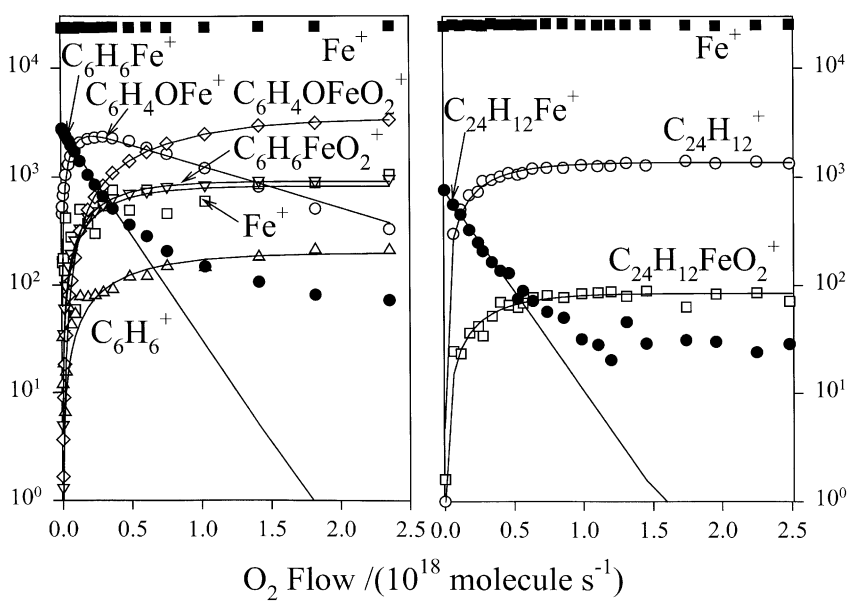

Fig. 6. Experimental data for the reactions of $C_6H_6Fe^+$ and $C_{24}H_{12}Fe^+$ with O_2. The solid lines represent a fit of the experimental data points with the solution of the system of differential equations appropriate for the observed sequential additions. The occurrence of reverse reactions has been neglected.

predominant (90%):

$$C_{24}H_{12}Fe^+ + O_2 \rightarrow C_{24}H_{12}{}^+ + FeO_2 \quad (8a)$$

$$C_{24}H_{12}Fe^+ + O_2 \rightarrow C_{24}H_{12}FeO_2{}^+ \quad (8b)$$

Reactions (7) and (8) both are fast, $k_7 \geq 1.8 \times 10^{-10}$ cm^3 molecule^{-1} s^{-1} and $k_8 = 2.7 \times 10^{-10}$ cm^3 molecule^{-1} s^{-1}. k_7 is a lower limit because of curvature in the decay of $C_6H_6Fe^+$ that we attribute to the occurrence of the reverse of the association reaction (7d).

The neutral species produced in reaction (8a) can be predicted from available thermodynamics to be FeO_2 and not $Fe + O_2$ or $FeO + O$. The occurrence of reaction (8a) with $Fe + O_2$ as neutral products can be calculated to be endothermic by 41.8 kcal mol^{-1} using a bond energy for Fe^+-$C_{24}H_{12}$ of 56.0 kcal mol^{-1} [18] and the ionization energies of Fe (7.9024 ± 0.0001 eV) [26] and $C_{24}H_{12}$ (7.29 ± 0.03 eV) [26]. DFT calculations have shown that formation of $FeO + O$ would require an additional 21 kcal mol^{-1} [37]. The same DFT calculations [37] indicate three possible stable isomers of FeO_2. These are, in order of increasing stability (where the energy relative to $Fe + O_2$ is given in parentheses): a bent "superoxo" addition product, FeOO ($\Delta E = -17$ kcal mol^{-1}), a cyclic peroxo adduct Fe(O_2) ($\Delta E = -27$ kcal mol^{-1}) and an oxidative insertion product, bent OFeO ($\Delta E = -64$ kcal mol^{-1}). Therefore, only the formation of the insertion product OFeO is exothermic in reaction (8a), with $\Delta H_r^\circ = -22.1$ kcal mol^{-1}.

The thermochemistry of the major channel leading to the elimination of water, reaction (7a), is not known because of the unknown identity of $FeC_6H_4O^+$. To gain insight into the structure of $FeC_6H_4O^+$ this ion was investigated using multi-collision CID. A CID profile obtained in Ar (0.094 Torr) at a flow of O_2 of 3.8×10^{18} molecule s^{-1} is shown in Fig. 7. The $FeC_6H_4O^+$ ion is seen to dissociate by loss of CO and subsequent loss of acetylene. A similar dissociation pattern was observed by Schröder et al. for the dissociation of a $C_6H_4OFe^+$ ion produced from the reaction of Fe^+ with dihydroxybenzene [38] and from the reaction of FeO^+ with phenol [39].

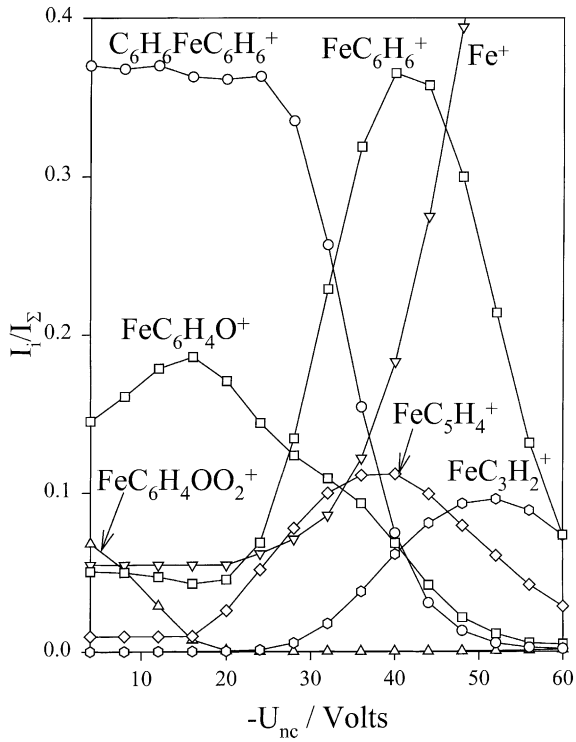

Fig. 7. Profile obtained for the multi-collision induced dissociation of $C_6H_4OFe^+$ in Ar at 0.094 Torr and at an O_2 flow of 3.8×10^{18} molecule s^{-1}.

Isotope-labeling experiments, extensive MS/MS studies and collision-induced dissociation measurements of ions with the same molecular formula but different structures generated by independent routes indicated the structure shown in Scheme 1 as the most possible structure for $FeC_6H_4O^+$ that loses CO upon collision-induced dissociation [39]. We propose that $FeC_6H_4O^+$ produced in reaction (7a) under our experimental conditions also has this structure.

The identity of the neutral product ($C_6H_6O_2$) in the reaction channel (7b) is also not known. Stoichiometric possibilities include the combinations of benzene and molecular oxygen, phenol and atomic oxygen, or 2,4-cyclopentadien-1-ylidene methanone

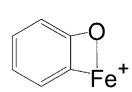

Scheme 1. Benzometalcycle $FeC_6H_4O^+$.

(C_6H_4O) and water or 1,2-dihydroxybenzene. Available thermochemical information [36] indicates that the most exothermic channel involves the generation of 1,2-dihydroxybenzene (catechol) ($\Delta H_r^\circ = -84.8 \pm 1.1$ kcal mol^{-1}). The formation of Fe^+ in channel (7b) is intriguing since this means that the sequence of reactions starting with the formation of $C_6H_6Fe^+$ from Fe^+ and neutral benzene followed by reaction (7b) constitutes a catalytic cycle in which the benzene ring is oxidized in the presence of iron cations that act as a catalyst.

$$Fe^+ + C_6H_6 \rightarrow C_6H_6Fe^+$$

$$\underline{C_6H_6Fe^+ + O_2 \rightarrow Fe^+ + (C_6H_6O_2)}$$

$$C_6H_6 + O_2 \rightarrow (C_6H_6O_2) \quad (9)$$

The occurrence of the minor channel (7c), the analogue of reaction (8a) is surprising, at least at first glance, since it is endothermic by 18 kcal mol^{-1}. The thermochemistry of this reaction is available because the binding energy D(Fe^+-benzene) is known, 51.1 kcal mol^{-1}, [6] as are the ionization energies of benzene (9.24378 ± 0.00007 eV), [26] and Fe (7.9024 ± 0.0001 eV), [26]. A likely source of $C_6H_6{}^+$ is excited $C_6H_6Fe^+$ ions that were not completely quenched by collisions with helium in their formation from Fe^+ and C_6H_6.

The O_2 addition reaction (7d) appears to be reversible and so contribute to the observed decay of $C_6H_6Fe^+$. The $C_6H_6FeO_2{}^+/C_6H_6Fe^+$ ratio plot indicates approach to equilibrium and that the oxygen is bound to $C_6H_6Fe^+$ by ca. 10 kcal mol^{-1}. The $C_{24}H_{12}FeO_2{}^+/C_{24}H_{12}Fe^+$ ratio plot behaves in a similar way with a similar O_2 binding energy for $C_{24}H_{12}Fe^+$.

We can compare our results for reaction (7) with observations obtained using ICR experiments in which ($C_6H_6Fe^+$) was produced from the reaction between $C_2H_4Fe^+$ and benzene that formally corresponds to ligand exchange [23]. The reaction between ($C_6H_6Fe^+$) and O_2 is reported to be fast under ICR conditions, 6.9×10^{-10} cm^3 molecule^{-1} s^{-1}, and the channels observed are completely different from those recorded under our experimental conditions:

$$(C_6H_6Fe^+) + O_2 \rightarrow C_5H_6OFe^+ + CO \quad (0.55) \quad (10a)$$

$$(C_6H_6Fe^+) + O_2 \rightarrow C_5H_4Fe^+ + CO + H_2O \quad (0.45) \quad (10b)$$

The loss of CO in both of these channels must involve considerable bond redisposition if ($C_6H_6Fe^+$) is a benzene adduct of Fe^+ and this is likely to require energy. It is interesting that the ion with the molecular formula $C_5H_4Fe^+$ is obtained in our CID experiments (see Fig. 7) from the dissociation of $C_6H_4OFe^+$ by loss of CO at an onset energy of around −20 V in argon buffer gas, indicating that the process requires significant collision energy which is not available under thermal conditions. Therefore, we must conclude that the $C_6H_6Fe^+$ reactant ion in the ICR experiments is either not thermalized or not properly identified.

4. Conclusions

The reactivity of thermalized $C_{24}H_{12}Fe^+$ and $C_6H_6Fe^+$ towards a set of neutral ligands has been investigated using the SIFT method. Rate coefficients have been measured for ion-molecule reactions involving these ligated ions and compared with results for the bare Fe^+. The kinetic measurements have revealed rate enhancement for ligation reactions of up to five orders of magnitude for the metal center upon coordination with both the benzene and coronene aromatic systems. The dependence of ligation kinetics on the number of degrees of freedom available for energy redisposition in the transient intermediate explains, at least in part, the observed enhancement.

Coordination numbers were derived from the extent of sequential reactivity observed for $C_6H_6Fe^+$ and $C_{24}H_{12}Fe^+$ and rationalized in terms of the modes of coordination of Fe^+ with the aromatic substrate and the ligand.

Bimolecular oxidation channels were observed to compete with ligation in the reactions of $C_6H_6Fe^+$ and $C_{24}H_{12}Fe^+$ with N_2O and O_2. The oxidation of

Fe^+ to form FeO^+ with N_2O can be catalyzed by the presence of benzene or coronene. Fe-atom abstraction to form FeO_2 was observed in the reactions with O_2. The $C_6H_6Fe^+$ adduct also eliminated water upon addition of O_2 to form a benzometalcycle $FeC_6H_4O^+$ cation and can initiate the Fe^+ catalyzed oxidation of benzene to 1,2-dihydroxybenzene (catechol).

The study reported here demonstrates that the kinetic method employed can be used to rationalize coordination patterns for metallo-aromatic cations by elucidating sequential ligation kinetics. Competing bimolecular channels can also be identified. The latter can be the consequence of metal-cation activation of the aromatic substrate and can result in the initiation of catalytic chemistry.

Acknowledgements

Continued financial support from the Natural Sciences and Engineering Research Council of Canada is greatly appreciated. As holder of a Canada Research Chair in Physical Chemistry, Diethard K. Bohme thanks the Canada Research Chair Program for its contributions to this research.

References

[1] J. Sunner, K. Nishizawa, P. Kerbale, J. Phys. Chem. 85 (1981) 1814.
[2] B.C. Guo, J.W. Purnell, A.W. Castelman, Chem. Phys. Lett. 168 (1990) 155.
[3] K.F. Willey, C.S. Yeh, D.L. Robbins, M.A. Duncan, J. Phys. Chem. 96 (1992) 9106.
[4] M. Lacoste, H. Rabaa, D. Astruc, A. Le Beuze, J. Saillard, G. Precigoux, C. Courseille, N. Ardoin, W. Bowyer, Organometallics 8 (1989) 2233.
[5] J.C. Ma, D.A. Dougherty, Chem. Rev. 97 (1997) 1303.
[6] C.W. Bauschlicher, H. Partridge, S.R. Langhoff, J. Phys. Chem. 96 (1992) 3273.
[7] F. Meyer, F.A. Khan, P.B. Armentrout, J. Am. Chem. Soc. 117 (1995) 9740.
[8] C. Yang, S.J. Klippenstein, J. Phys. Chem. A 103 (1999) 1094.
[9] D.A. Dougherty, Science 271 (1996) 163.
[10] P. Weis, P.R. Kemper, M.T. Bowers, J. Phys. Chem. 101 (1997) 8207.
[11] T. Kurikawa, H. Takeda, M. Hirano, K. Judai, T. Arita, S. Nagao, A. Nakajima, K. Kaya, Organometallics 18 (1999) 1430.
[12] C. Janiak, H. Hemling, Chem. Ber. 127 (1994) 1251.
[13] B.P. Pozniak, R.C. Dunbar, J. Am. Chem. Soc. 119 (1997) 10439.
[14] D.K. Bohme, Chem. Rev. 92 (1992) 1487.
[15] P. Boissel, Astron. Astrophys. 285 (1994) L33.
[16] C.W. Bauschlicher, S.R. Langhoff, H. Partridge, in: B.S. Freiser (Ed.), Organometallic Ion Chemistry, Kluwer Academic Publishers, Dordrecht, 1996.
[17] J.W. Buchanan, G.A. Grieves, J.E. Reddic, M.A. Duncan, Int. J. Mass Spectrom. 182/183 (1999) 323.
[18] S.J. Klippenstein, C. Yang, Int. J. Mass Spectrom. 210 (2000) 253.
[19] B. Chaudret, A. Le Beuze, H. Rabaa, Y. Saillard, G. Serra, New J. Chem. 15 (1991) 791.
[20] J.M. Schulman, R.L. Disch, J. Phys. Chem. A 101 (1997) 9176.
[21] V. Baranov, D.K. Bohme, Int. J. Mass Spectrom. Ion Process. 149/150 (1995) 543.
[22] D. Stöckigt, H. Schwarz, Chem. Ber. 127 (1994) 2499.
[23] D. Schröder, H. Schwarz, Angew. Chem. Int. Ed. Engl. 32 (1993) 1420.
[24] D. Caraiman, G.K. Koyanagi, L.T. Scott, D.V. Preda, D.K. Bohme, J. Am. Chem. Soc. 123 (2001) 8573.
[25] G.I. Mackay, G.D. Vlachos, D.K. Bohme, H.I. Schiff, Int. J. Mass Spectrom. Ion Phys. 36 (1980) 259.
[26] S.G. Lias, J.E. Bartmess, J.F. Liebman, J.L. Holmes, R.D. Levin, W.G. Mallard, Ion energetics data, in: W.G. Mallard, P.J. Linstrom (Eds.), NIST Chemistry WebBook, NIST Standard Reference Database Number 69, February 2000, National Institute of Standards and Technology, Gaithersburg MD, 20899 (http://webbook.nist.gov).
[27] P.M. Hierl, A.F. Ahrens, M.J. Henchman, A.A. Viggiano, J.F. Paulson, Int. J. Mass Spectrom. Ion Process. 81 (1987) 101.
[28] V. Baranov, D.K. Bohme, Int. J. Mass Spectrom. Ion Process. 154 (1996) 71.
[29] V. Baranov, G. Javahery, A.C. Hopkinson, D.K. Bohme, J. Am. Chem. Soc. 117 (1995) 12801.
[30] V. Baranov, H. Becker, D.K. Bohme, J. Phys. Chem. A 101 (1997) 5137.
[31] R.K. Milburn, V.I. Baranov, A.C. Hopkinson, D.K. Bohme, J. Phys. Chem. A 102 (1998) 9803.
[32] T. Su, J. Chesnavich, J. Chem. Phys. 76 (1982) 5183.
[33] A. Good, Trans. Faraday Soc. 67 (1971) 3495.
[34] R. Schulz, P.B. Armentrout, J. Phys. Chem. 97 (1993) 596.
[35] R.C. Weast, M.J. Astle, CRC Handbook of Chemistry and Physics, 67th ed., CRC Press, Inc., Boca Raton, FL, 1986/1987.
[36] S.G. Lias, J.E. Bartmess, J.F. Liebmanm, J.L. Holmes, R.D. Levin, W.G. Mallard, J. Phys. Chem. Ref. Data 17 (Suppl. 1) (1988).
[37] L. Andrews, G.V. Chertihin, A. Ricca, C.W. Bauschlicher, J. Am. Chem. Soc. 118 (1996) 467.
[38] D. Schröder, W. Zummack, H. Schwarz, Organometallics 12 (1993) 1079.
[39] M. Brönstrup, D. Schröder, H. Schwarz, Chem. Eur. J. 6 (2000) 91.